Supplement of Improving the CLASSIC (v1.8) Snow Model to Better Simulate Arctic Snowpacks

Mickaël Lalande[1, 2], Alexandre Roy[1, 2], Libo Wang[3], Diana Verseghy[4,*], Vincent Vionnet[5], Florent Dominé[2, 6, 7], and Christophe Kinnard[1, 2]

[1]Centre for Research on Watershed-Aquatic Ecosystem Interactions, Department of Environmental Sciences, Université du Québec à Trois-Rivières, Trois-Rivières, QC, Canada
[2]Centre for Northern Studies, Université Laval, Québec, QC, Canada
[3]Climate Research Division, Environment and Climate Change Canada, Toronto, ON, Canada
[4]Formerly at Climate Research Division, Environment and Climate Change Canada, Toronto, ON, Canada
[5]Meteorological Research Division, Environment and Climate Change Canada, Dorval, QC, Canada
[6]Takuvik Joint International Laboratory, Université Laval (Canada) and CNRS-INSU (France), Québec, QC, Canada
[7]Department of Chemistry, Université Laval, Québec, QC, Canada
[*]retired

Correspondence: Mickaël Lalande (mickael.lalande.phd@gmail.com)

Contents

1 Further details on in situ stations

Table S1. Sites setup. Soil color index (SOCI) is derived from the SoilGrids250m dataset (Hengl et al., 2017), and permeable soil depth (SDEP) is based on Shangguan et al. (2017). The proportions of C3 and C4 grasses are derived from Wang et al. (2006). fcancmx corresponds to the CTEM PFTs (BdlSh: broadleaf shrubs, BdlDCoSh: broadleaf deciduous cold shrub), respectively. The remaining percentage of fcancmx is attributed to bare ground. ZRFH and ZRFM correspond to the reference heights at which energy (air temperature and specific humidity) and momentum (wind) variables are provided. See Table 1 for site abbreviations and Sect. 2.1 of the main article for more information.

Site (short)	SDEP (m)	SOCI	fcancmx	ZRFH (m)	ZRFM (m)	Comment
cdp	13.37	15	∼98 % Grass C3 ∼2 % Grass C4	1.5	10	Grassy meadow bordered by coniferous forest. Soil: Lejeune et al. (2019).
rme	23.87	14	∼100 % Grass C3	3.0	3.0	Sheltered grassy site in an aspen and fir grove. High organic content in surface soils and 50 cm of silty clay (42 % clay, 42 % silt) overlying clay (50 % clay, 40 % silt).
snb	5.87	17	∼68 % Grass C3 ∼2 % Grass C4	3.8	4.0	Alpine tundra with thin soils and exposed bedrock.
swa	5.87	17	∼98 % Grass C3 ∼2 % Grass C4	3.4	3.8	Sheltered meadow surrounded by subalpine forest. Colluvium.
sap	25.34	19	100 % Grass C3	1.5	1.5	Urban short grass site with frequent deposition of atmospheric aerosols. Clay soil.
sod	23.76	14	100 % Grass C3	2.0	2.0	Small clearing in a pine plantation with sandy loam soil. Wind speed and radiation are measured above the canopy height, so forcing data have been adjusted for the sheltering of the clearing.
wfj	4.59	13	-	4.5	5.5	Artificially drained moraine containing clay sediments overlain by serpentine rocks of varying sizes up to 20 cm diameter.
byl	4.96	6	100 % Grass C3	2.3	2.3	The site is a low-center polygon, with herb tundra and no erect vegetation.
umt	7.23	13	50 % BdlDCoSh	2.3	10.0	Lichen and shrub tundra. Soil composition is 95 % sand and 5 % silt (Gagnon et al., 2019; Lackner et al., 2022).
tvc	9.84	16	60 % Sedge 5 % BdlEvgSh 28 % BdlDCoSh	2.0	4.0	Southern Arctic tundra site, erect-shrub tundra, tundra dominated by low shrubs < 40 cm, continuous permafrost. Mineral soil 35 % sand / 40 % clay (Marsh et al., 2010).

Table S2. The sites' initialization soil texture consists of a combination of site information and satellite data (Hengl et al., 2017), except for cdp where soil texture was derived from Lejeune et al. (2019) (see: https://github.com/mickaellalande/SnowC2/blob/main/CLASSIC/in_situ/SnowMIP/FR-Cdp_test/init/soil_properties_Lejeune2019.ipynb for more details; last access 24 March 2024). Flags -2 and -3 represent peat and bedrock layers, respectively. The 20 soil layer thicknesses (m) of the model are: [0.1, 0.1, 0.1, 0.1, 0.1, 0.1, 0.1, 0.1, 0.1, 0.1, 0.2, 0.3, 0.4, 0.5, 1., 3., 5., 15., 30., 5.] and the bottom depths of the layers (m) are [0.1, 0.2, 0.3, 0.4, 0.5, 0.6, 0.7, 0.8, 0.9, 1. , 1.2, 1.5, 1.9, 2.4, 3.4, 6.4, 11.4, 26.4, 56.4, 61.4]. The column notebook links to the detailed method used for each site. The footnotes link to the detailed method used for each site. See Table 1 for site abbreviations and Sect. 2.1 in the main article for more information.

Site (short)	SAND (%)	CLAY (%)	ORGM (%)
cdp[1]	[28.2, 28.8, 28.6, 29.9, 28.9, 25.9, 28.6, 29.3, 24.4, 24.4, 24.4, 24.4, 24.4, 24.4, 24.4, 24.4, 24.4, 24.4, -3., -3.]	[25.8, 27.2, 32.5, 33.4, 31.9, 32.8, 31.0, 29.7, 31.1, 31.1, 31.1, 31.1, 31.1, 31.1, 31.1, 31.1, 31.1, 31.1, 0. , 0.]	[6.7, 4.3, 2.2, 0.8, 0.5, 0.4, 0.3, 0.3, 0.4, 0.4, 0.4, 0.4, 0.4, 0.4, 0.4, 0.4, 0.4, 0., 0.]
rme[2]	[16., 16., 15.9, 15.6, 15.3, 15.0, 14.7, 14.4, 14.1, 13.8, 13.3, 12.6, 11.5, 10.2, 10.2, 10.2, 10.2, 10.2, -3., -3.]	[42. , 42. , 42.1, 42.5, 42.9, 43.3, 43.7, 44.1, 44.5, 44.9, 45.5, 46.5, 47.9, 49.7, 49.7, 49.7, 49.7, 49.7, 0. , 0.]	[10., 4.2, 0., 0., 0., 0., 0., 0. 0. 0. 0. 0. 0. 0., 0., 0., 0., 0. , 0., 0.]
snb[3]	[-2., 29.6, 29.6, 28.1, 38.4, 37.7, 38.4, 37.7, 36.9, 36.2, 35.8, 33.9, 31.3, 27.9, 27.9, 27.9, -3., -3., -3., -3.]	[0., 29.6, 29.6, 28.1, 20.4, 19.7, 18.7, 17.9, 17.2, 16.4, 15.1, 13.2, 10.6, 7.2, 7.2, 7.2, 0., 0., 0., 0.]	[0., 1.9, 1.9, 1.8, 2.5, 2.5, 1.9, 1.8, 1.8, 1.7, 1.5, 1.4, 1.2, 1.0, 1.0, 1.0, 0., 0., 0., 0.]
swa[4]	70., 70., 70., 70., 60.1, 60.1, 61.6, 61.6, 61.6, 61.6, 62.4, 62.4, 62.4, 62.4, 62.4, 62.4, -3., -3., -3., -3.]	[5., 5., 5., 5., 9.6, 9.6, 9.4, 9.4, 9.4, 9.4, 9.1, 9.1, 9.1, 9.1, 9.1, 9.1, 0., 0., 0., 0.]	[2., 0.8, 0., 0., 1.6, 1.6, 1.1, 1.1, 1.1, 1.1, 1.0, 1.0, 1.0, 1.0, 1.0, 1.0, 0., 0., 0., 0.]
sap[5]	[20., 20., 20., 20., 30.0, 30.0, 30.4, 30.4, 30.4, 30.4, 30.9, 30.9, 30.9, 30.9, 30.9, 30.9, 30.9, 30.9, -3., -3.]	[60., 60., 60., 60., 42.0, 42.0, 42.1, 42.1, 42.1, 42.1, 41.7, 41.7, 41.7, 41.7, 41.7, 41.7, 41.7, 41.7, 0., 0.]	[2., 0.8, 0., 0., 3.4, 3.4, 2.8, 2.8, 2.8, 2.8, 2.8, 2.8, 2.8, 2.8, 2.8, 2.8, 2.8, 0., 0.]
sod[6]	[70., 70., 70., 70., 63.2, 63.2, 63.7, 63.7, 63.7, 63.7, 63.9, 63.9, 63.9, 63.9, 63.9, 63.9, 63.9, 63.9, -3., -3.]	[10., 10., 10., 10., 7.6, 7.6, 7.6, 7.6, 7.6, 7.6, 7.6, 7.6, 7.6, 7.6, 7.6, 7.6, 7.6, 7.6, 0., 0.]	[2., 0.8, 0., 0., 4.5, 4.5, 4.0, 4.0, 4.0, 4.0, 4.0, 4.0, 4.0, 4.0, 4.0, 4.0, 4.0, 4.0, 0., 0.]
wfj[7]	[90., 50., 20., 20., 34.1, 34.1, 35.5, 35.5, 35.5, 35.5, 36.1, 36.1, 36.1, 36.1, 36.1, 36.1, -3., -3., -3., -3.]	[5., 36.4, 60., 60., 35.2, 35.2, 35.3, 35.3, 35.3, 35.3, 35.4, 35.4, 35.4, 35.4, 35.4, 35.4, 0., 0., 0., 0.]	[0., 0., 0., 0., 4.2, 4.2, 3.3, 3.3, 3.3, 3.3, 2.9, 2.9, 2.9, 2.9, 2.9, 2.9, 0., 0., 0., 0.]
byl[8]	[-2., 43.5, 63.5, 54.4, 54.4, 54.4, 54.6, 54.6, 54.6, 54.6, 54.2, 54.2, 54.2, 54.2, 54.2, 54.2, -3., -3., -3., -3.]	[0., 0., 0.1, 7.5, 7.5, 7.5, 7.6, 7.6, 7.6, 7.6, 7.4, 7.4, 7.4, 7.4, 7.4, 7.4, 0., 0., 0., 0.]	[0., 1.5, 1.5, 6.4, 6.4, 6.4, 6.0, 6.0, 6.0, 6.0, 5.7, 5.7, 5.7, 5.7, 5.7, 5.7, 0., 0., 0., 0.]
umt[9]	[-2., 95., 95., 95., 95., 95., 95., 95., 95., 95., 95., 95., 95., 95., 95., 95., -3., -3., -3.]	[0., 0., 0., 0., 0., 0., 0., 0., 0., 0., 0., 0., 0., 0., 0., 0., 0., 0., 0., 0.]	[1., 0.25, 0.2, 0.2, 0.2, 0.2, 0.2, 0.2, 0.2, 0.2, 0.2, 0.2, 0.2, 0.2, 0.2, 0.2, 0.2, 0., 0., 0.]
tvc[10]	[-2, 35, 35, 35, 35, 35, 35, 35, 35, 35, 35, 35, 35, 35, 35, 35, 35, 35, 35, 35]	[40.0, 40.0, 40.0, 40.0, 40.0, 40.0, 40.0, 40.0, 40.0, 40.0, 40.0, 40.0, 40.0, 40.0, 40.0, 40.0, 40.0, 40.0, 40.0, 40.0]	[8.0, 8.0, 8.0, 8.0, 8.0, 8.0, 8.0, 8.0, 8.0, 8.0, 8.0, 8.0, 8.0, 8.0, 8.0, 8.0, 8.0, 8.0, 8.0, 8.0]

[1] https://github.com/mickaellalande/SnowC2/blob/main/CLASSIC/in_situ/SnowMIP/cdp/init/init_cdp-Ref.ipynb (last access: 9 October 2025)

[2] https://github.com/mickaellalande/SnowC2/blob/main/CLASSIC/in_situ/SnowMIP/rme/init/init_rme-Ref.ipynb (last access: 9 October 2025)

[3] https://github.com/mickaellalande/SnowC2/blob/main/CLASSIC/in_situ/SnowMIP/snb/init/init_snb-Ref.ipynb (last access: 9 October 2025)

[4] https://github.com/mickaellalande/SnowC2/blob/main/CLASSIC/in_situ/SnowMIP/swa/init/init_swa-Ref.ipynb (last access: 9 October 2025)

[5] https://github.com/mickaellalande/SnowC2/blob/main/CLASSIC/in_situ/SnowMIP/sap/init/init_sap-Ref.ipynb (last access: 9 October 2025)

[6] https://github.com/mickaellalande/SnowC2/blob/main/CLASSIC/in_situ/SnowMIP/sod/init/init_sod-Ref.ipynb (last access: 9 October 2025)

[7] https://github.com/mickaellalande/SnowC2/blob/main/CLASSIC/in_situ/SnowMIP/wfj/init/init_wfj-Ref.ipynb (last access: 9 October 2025)

[8] https://github.com/mickaellalande/SnowC2/blob/main/CLASSIC/in_situ/SnowArctic/byl/init/init_byl-peat_30min_ext.ipynb (last access: 9 October 2025)

[9] https://github.com/mickaellalande/SnowC2/blob/main/CLASSIC/in_situ/SnowArctic/umt/init/init_umt-Ref.ipynb (last access: 9 October 2025)

[10] https://github.com/mickaellalande/SnowC2/blob/main/CLASSIC/in_situ/SnowArctic/tvc/init/init_tvc-Ref_1peat.ipynb (last access: 9 October 2025)

Table S3. Variables used at the sites during the time periods considered in this study. SWE and snow depth include automatic (auto) and manual (man) measurements. See Table 1 for site abbreviations and Sect. 2.1 for more information.

Site (short)	SWE (auto)	SWE (man)	Snow depth (auto)	Snow depth (man)	Albedo	Surface temperature	Soil temperature	Soil moisture
cdp	x	x	x	x	x	x	x	
rme	x	x	x	x			x	
snb		x	x	x	x	x	x	
swa		x	x	x	x	x	x	
sap		x	x	x	x	x		
sod	x	x	x	x			x	
wfj		x	x	x	x	x	x	
byl		x	x	x		x	x	x
umt		x	x	x			x	x
tvc		x	x	x			x	x

2 Relative to specific humidity conversion

CLASSIC uses specific humidity as an input variable, whereas only relative humidity is provided at some sites (Umiujaq and TVC). The relative humidity RH (%) is the ratio of the partial pressure of water vapor in an air-water mixture e (Pa) to the saturated vapor pressure of water at a given temperature e_s (Pa):

$$RH = \frac{m_v}{m_{vs}} = \frac{e}{e_s}, \tag{1}$$

with m_v and m_{vs} the mass of water vapor and the mass of saturated water vapor, respectively. The specific humidity q (kg kg^{-1}) is the mass of water vapor in the total mass of air:

$$q = \frac{\rho_v}{\rho_d + \rho_v} = \frac{m_v}{m_d + m_v}, \tag{2}$$

with ρ_d and ρ_v the density of dry air and the density of water vapor, respectively (kg m^{-3}).

To calculate the saturation vapor pressure of water, Eq. (17) of Huang (2018) is used (even for temperatures lower than 0 °C, as the relative humidity sensors at Umiujaq and TVC are calibrated only with respect to water):

$$e_s = \frac{\exp\left(34.494 - \frac{4924.99}{T+237.1}\right)}{(T+105)^{1.57}} \left(\mathrm{T} > 0^{\circ}\mathrm{C}\right), \tag{3}$$

with T being the temperature in °C and e_s in Pa.

Then the water vapor pressure was derived with: $e = \frac{RH}{e_s}$, which allows the absolute humidity a (kg m^{-3}) to be derived with the gas equation of state $eV = n_v RT$ with $n_v = \frac{m_v}{M_v}$, where V is the volume considered, $R = 8.31446$ J K^{-1} mol^{-1} is the molar mass constant, n_v is the amount of water vapor (mol), $M_v = 0.0180153$ kg mol^{-1} the molecular molar mass of water, and T the temperature (K):

$$a = \rho_v = \frac{m_v}{V} = \frac{eM_v}{RT}. \tag{4}$$

Finally, the total density of air has to be evaluated to get to the specific humidity:

$$\rho_d + \rho_v = \frac{p_d M_d + eM_v}{RT}, \tag{5}$$

with $p_d = P - e$ the partial pressure of dry air (Pa), $M_d = 0.028965$ kg mol^{-1} the molecular molar mass of dry air, and P the total air pressure (Pa).

The numerical implementation of this computation can be found at: https://github.com/mickaellalande/SnowC2/blob/main/CLASSIC/in_situ/SnowArctic/tvc/forcing/forcing_tvc_to_SnowMIP_correct_SH.ipynb (last access: 10 October 2025).

3 Snowfall rate sensitivity at Trail Valley Creek

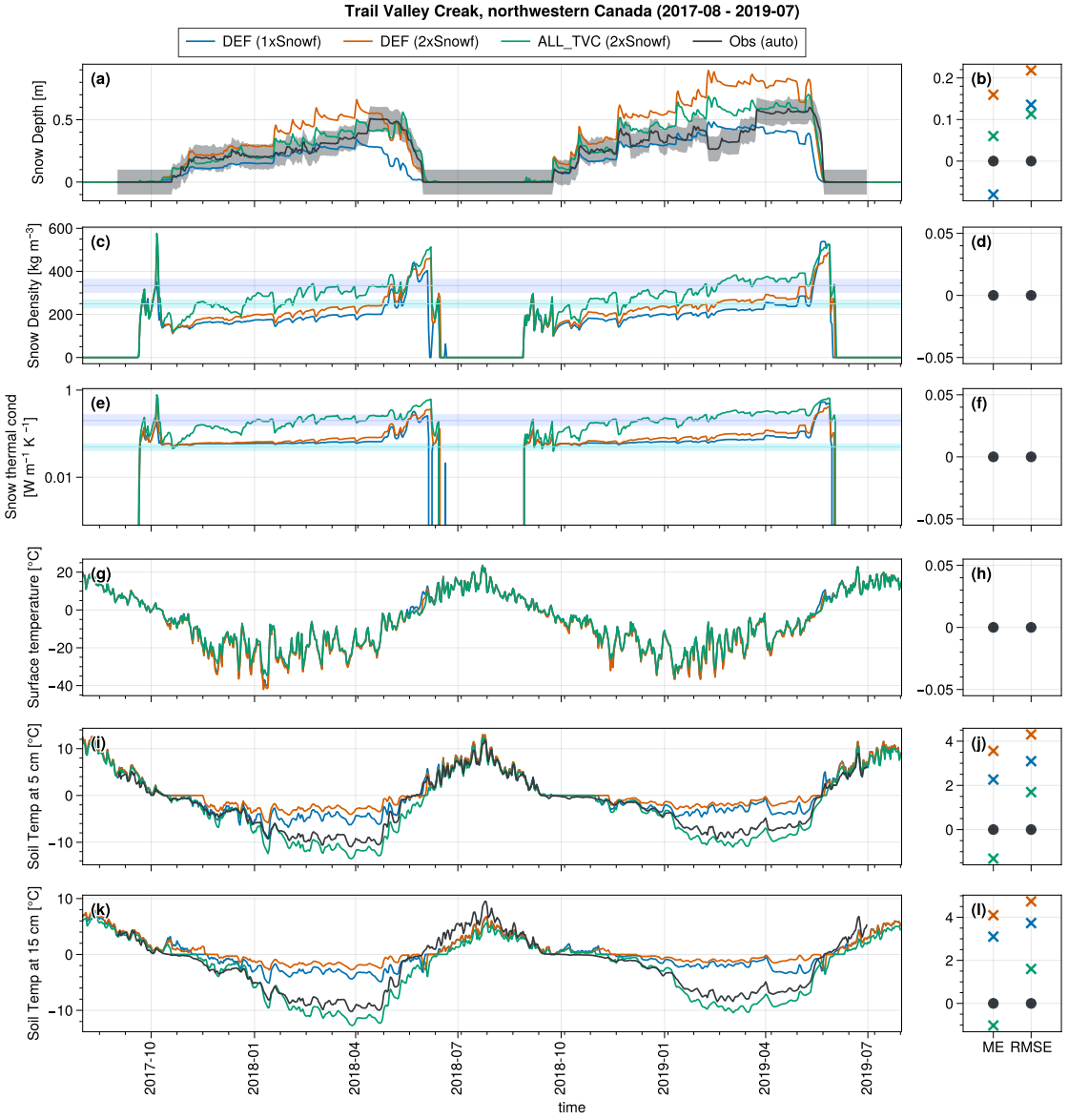

Figure S1. Time series of snow depth (a), snow density (c), snow thermal conductivity (e), snow surface temperature (g), and soil temperatures at 5 and 15 cm (m and k) at TVC from September 2017 to June 2019. Simulations are shown for the *DEF* experiment using the original snowfall rate at TVC (blue line) and for the *DEF* and *TVC_ALL* experiments using the doubled snowfall rate applied in this study (orange and green lines, respectively; see Table 2 of the main text for experiment descriptions). Automatic observations are shown in black. Black shading indicates measurement uncertainties derived at Col de Porte (Lejeune et al., 2019) and is provided as an indicative reference. Dark and light blue horizontal shadings in panels (c) and (e) represent the mean snow densities and thermal conductivities of wind slab and depth hoar, respectively, derived from multiple snow pits around the site (Dutch et al., 2022, Table 2). Right-hand panels show the mean error and RMSE over the 2017–2019 period, computed for snow depths exceeding 10 cm.

4 Code implementation

All the code implementations are available at: https://github.com/mickaellalande/SnowC2-CLASSIC-1D-model/tree/v0.1.0 (Lalande, 2026). Our developments were based on the CLASSIC development version [commit SHA: 57f7993ac417751c71bb1d815c531b9a8f4bf926, https://gitlab.com/jormelton/classic/-/commit/57f7993ac417751c71bb1d815c531b9a8f4bf926, last access: 6 January 2026].

4.1 Snow model: physics improvements

4.1.1 Thermal conductivity at the top of the first soil layer

To solve the issue described in Sect. 2.3.1 of the main text, *ZERO* is passed to *soilHeatFluxPrep.f90* instead *ZSNOW* to the subfractions without snow in *energyBudgetDriver.f90*:

- CANOPY OVER BARE GROUND: https://github.com/mickaellalande/SnowC2-CLASSIC-1D-model/blame/SnowC2-1D/src/energyBudgetDriver.f90#L1357 (last access: 21 December 2025)
- BARE GROUND: https://github.com/mickaellalande/SnowC2-CLASSIC-1D-model/blame/SnowC2-1D/src/energyBudgetDriver.f90#L1556 (last access: 21 December 2025)

See more information at: https://gitlab.com/cccma/classic/-/issues/119 (last access: 21 December 2025).

4.1.2 Bottom snow temperature

In *snowTempUpdate.f90* (https://github.com/mickaellalande/SnowC2-CLASSIC-1D-model/blob/SnowC2-1D/src/snowTempUpdate.f90#L152; last access: 21 December 2025), the computation of the bottom snow temperature $T_{s,b}$ has been modified from:

$$T_{s,b} = \frac{d_s T_s + d_1 T_1}{d_s + d_1} \tag{6}$$

to

$$T_{s,b} = \frac{\frac{T_s}{d_s} + \frac{T_1}{d_1}}{\frac{1}{d_s} + \frac{1}{d_1}}, \tag{7}$$

where T_1 is the first soil layer temperature, T_s the snow temperature, and d_1 and d_s their respective thickness.

4.1.3 Windless exchange coefficient

A windless transfer coefficient E_0 is introduced into the sensible heat flux Q_H (W m $^{-2}$) calculation of 2 W m $^{-2}$ K^{-1} during stable atmospheric conditions over non-vegetated areas (i.e., over bare ground or when snow entirely buries the vegetation), as follows in *energBalNoVegSolve.f90*:

$$Q_H = (\rho_{\text{air}}\, c_P\, C_H\, U + E_0)\,(T_s - \theta_a)\,, \tag{8}$$

where ρ_{air} is the density of air (kg m^{-3}), c_P is the specific heat capacity of air (set to 1.00464×10^3 J kg^{-1} K^{-1} in CLASSIC), C_H is the surface drag coefficient (unitless), U the wind speed at reference height (m s^{-1}), T_s the surface temperature (K), and θ_a the potential air temperature at the reference height (K). E_0 is set to 2 W m^{-2} K^{-1} when $T_s < \theta_a$ (i.e., for atmospheric stable condition) and 0 W m^{-2} K^{-1} otherwise. See Brown et al. (2006) their Fig. 11 for more details. The details of the implementation are described below:

- Set $E_0 = 2$ W m^{-2} K^{-1} if there is snow: https://github.com/mickaellalande/SnowC2-CLASSIC-1D-model/blame/SnowC2-1D/src/energBalNoVegSolve.f90#L269 (last access: 21 December 2025)
- Add it to the sensible heat flux (last access: 21 December 2025; already coded by Ross Brown; see paper above):
  - https://github.com/mickaellalande/SnowC2-CLASSIC-1D-model/blob/SnowC2-1D/src/energBalNoVegSolve.f90#L594
  - https://github.com/mickaellalande/SnowC2-CLASSIC-1D-model/blob/SnowC2-1D/src/energBalNoVegSolve.f90#L896

4.2 Snow model: Arctic adaptations

4.2.1 Blowing-snow sublimation losses

The blowing-snow sublimation loss parameterization of Gordon et al. (2006) is implemented:

$$Q_s = 0.0018 \left(\frac{T_0}{T_{\text{air}}}\right)^4 U_t \, \rho_a \, q_{si} \, (1 - RH_i) \left(\frac{U_{10}}{U_t}\right)^{3.6}, \quad \text{for } U_{10} > U_t \text{ and } T_{\text{air}} < T_0, \tag{9}$$

with:

$$U_t = 6.98 + 0.0033 \, (T_{\text{air}} - 245.88)^2, \tag{10}$$

where U_t [m s^{-1}] is the threshold wind speed at 10 m for the initiation of blowing snow, T_{air} is the near-surface air temperature [K], T_0 is the freezing point of water (defined as 273.16 °K in CLASSIC), ρ_a is the density of air [kg m^{-3}], q_{si} is the saturation specific humidity of ice at reference height [kg kg^{-1}], RH_i is the relative humidity with respect to ice [fraction], U_{10} is the wind speed at 10 m above the snow surface [m s^{-1}]. This equation is only applied over bare ground subareas covered with snow (i.e., over bare ground and when snow buries the vegetation). The blowing-snow sublimation losses from the intercepted snow on the canopy are not considered. The details of the implementation are described below:

- Implementation of the Gordon et al. (2006)'s parameterization in a new file: *snowWindSublimation.f90* (https://github.com/mickaellalande/SnowC2-CLASSIC-1D-model/blob/SnowC2-1D/src/snowWindSublimation.f90; last access: 21 December 2025)
- 10 m wind speed adjustment in *energyBudgetDriver.f90* (https://github.com/mickaellalande/SnowC2-CLASSIC-1D-model/blob/SnowC2-1D/src/energyBudgetDriver.f90#L1153; last access: 21 December 2025)

- Blowing-snow sublimation loss rate added to the evaporation flux in *energBalNoVegSolve.f90* (last access: 21 December 2025):
  - https://github.com/mickaellalande/SnowC2-CLASSIC-1D-model/blob/SnowC2-1D/src/energBalNoVegSolve.f90#L600
  - https://github.com/mickaellalande/SnowC2-CLASSIC-1D-model/blob/SnowC2-1D/src/energBalNoVegSolve.f90#L902

Ultimately, it may be preferable to distinguish blowing-snow sublimation losses from evaporation, which is treated as a component of the surface energy budget. Indeed, blowing-snow sublimation losses primarily occur in the lower atmospheric layers rather than at the surface. Consequently, including this process in the surface energy balance risks misallocating the associated latent cooling to the surface rather than the near-surface atmosphere (Dharmadasa et al., 2024). This issue will be addressed in future work.

4.2.2 Snow compaction

Fresh snow density (not modified) in *atmosphericVarsCalc.f90* (https://github.com/mickaellalande/SnowC2-CLASSIC-1D-model/blob/SnowC2-1D/src/atmosphericVarsCalc.f90#L135; last access: 21 December 2025)

Maximum snow density

The snow density ρ_s in CLASSIC increases exponentially towards a maximum snow density $\rho_{\max}$ as follows:

$$\rho_s(t+1) = [\rho_s(t) - \rho_{\max}] \exp\left(-\frac{0.01\Delta t}{3600}\right) + \rho_{\max}, \tag{11}$$

with:

$$\rho_{\max} = 450 - \frac{204.7}{d_s}\left[1.0 - \exp\left(-\frac{d_s}{0.673}\right)\right] \quad \text{for } T_s < 0^\circ\text{C and,} \tag{12}$$

$$\rho_{\max} = 700 - \frac{204.7}{d_s}\left[1.0 - \exp\left(-\frac{d_s}{0.673}\right)\right] \quad \text{for } T_s = 0^\circ\text{C,} \tag{13}$$

where d_s is the snow depth [m], T_s the snow temperature [°C], and Δt the model time step [s]. The maximum snow density formulations are based on Tabler et al. (1990), with additional temperature threshold and enhanced settling rates determined empirically (Brown et al., 2006, unpublished manuscript, 2001) (https://www.dropbox.com/scl/fo/iu8l96afrllug7qs24qwu/ALwo3FkohrOK6Pl52W8ULDg?rlkey=bh5od4983961yef5x99zzpugk&st=j2xsh20z&dl=0; last access: 21 December 2025).

The maximum snow density for dry snow (Eq. 12) is modified with the addition of a dependence on the wind speed:

$$\rho_{\max} = 430 - \frac{204.7}{d_s}\left[1.0 - \exp\left(-\frac{d_s}{0.673}\right)\right] \quad \text{for } T_s < 0^\circ\text{C and } U < 2.5\ \text{m s}^{-1}\ (= \rho_{\text{no wind}}) \text{ and,} \tag{14}$$

$$\rho_{\max} = \rho_{\text{no wind}} + (\rho_{\text{wind}} - \rho_{\text{no wind}}) \exp\left[-\frac{(d_s - d_0)^2}{2\sigma^2}\right] \quad \text{for } T_s < 0^\circ\text{C and } U \geq 2.5\ \text{m s}^{-1}$$

$$= 430 - \frac{204.7}{d_s}\left[1.0 - \exp\left(-\frac{d_s}{0.673}\right)\right]\left\{1 - \left[1 - \exp\left(-\frac{U}{U_0}\right)\right]\exp\left[-\frac{(d_s - d_0)^2}{2\sigma^2}\right]\right\}, \tag{15}$$

with:

$$\rho_{\text{wind}} = 430 - \frac{204.7}{d_s}\left[1.0 - \exp\left(-\frac{d_s}{0.673}\right)\right]\exp\left(-\frac{U}{U_0}\right), \tag{16}$$

where U is the wind speed at 2 m above the snowpack [m s $^{-1}$], $U_0 = 2.5$ m s $^{-1}$ (or 3.5 m s $^{-1}$ for the TVC adjusted version; see Sects. 2.5 and 2.6 in the main text), $d_0 = 0.8$ m, and $\sigma = 1.0$ m. The constant 450 is reduced to 430 to better fit the observations across all sites, given the increased wind compaction during strong wind events. The wind-induced compaction is only applied over the bare ground subfraction (i.e., over non-vegetated subareas and/or when the snow entirely buries the vegetation) as we consider that there is no further snow compaction within the canopy. Over the vegetated subarea $\rho_{\text{no wind}}$ (Eq. 14) is maintained regardless of the wind speed. We adjust the wind speed provided at specific measurement heights to 2 m above the snowpack in the model using a logarithmic wind profile (Sect. 5). For wet snow, Eq. 13 is kept unchanged.

The implementation is described below:

- Implementation of the new maximum snow density: https://github.com/mickaellalande/SnowC2-CLASSIC-1D-model/blob/SnowC2-1D/src/snowProcesses.f90#L167 (last access: 21 December 2025)
- 2 m wind speed adjustment: https://github.com/mickaellalande/SnowC2-CLASSIC-1D-model/blob/SnowC2-1D/src/waterBudgetDr f90#L653 (last access: 21 December 2025)
- *snowAging* call over the snow cover ground: https://github.com/mickaellalande/SnowC2-CLASSIC-1D-model/blob/SnowC2-1D/src/waterBudgetDriver.f90#L661 (last access: 9 January 2026)
- *snowAging* call for the canopy snow subarea (pass *ZERO* for the wind speed within the canopy, as we consider that there is no further snow compaction due to wind within the canopy): https://github.com/mickaellalande/SnowC2-CLASSIC-1D-model/blob/SnowC2-1D/src/waterBudgetDriver.f90#L576 (last access: 9 January 2026)

4.2.3 Snow thermal conductivity

The current Sturm et al. (1997) snow thermal conductivity parameterization:

$$\lambda_s = \begin{cases} 0.234 \times 10^{-3}\,\rho_s + 0.023, & \rho_s < 156\ \text{kg m}^{-3}, \\ 3.233 \times 10^{-6}\,\rho_s^2 - 1.01 \times 10^{-3}\,\rho_s + 0.138, & \rho_s \geq 156\ \text{kg m}^{-3}, \end{cases}$$

was replaced with the Calonne et al. (2011)'s one:

$$\lambda_s = 2.5 \times 10^{-6}\,\rho_s^2 - 1.23 \times 10^{-4}\,\rho_s + 0.024, \tag{17}$$

with λ_s the snow thermal conductivity [W m $^{-1}$ K $^{-1}$], and ρ_s the snow density [kg m $^{-3}$]. The implementation of the new snow thermal conductivity can be found here: https://github.com/mickaellalande/SnowC2-CLASSIC-1D-model/blob/SnowC2-1D/src/energyBudgetPrep.f90#L666 (last access: 22 December 2025)

5 Logarithmic wind profile

To apply the new parameterizations to compute the maximum snow density for dry snow (Eqs. 14, 15, and 16), the wind speed is considered at 2 m above the snowpack. We use the following logarithmic profile:

$$U(z) = \frac{U_*}{\kappa} \ln\left(\frac{z}{z_0}\right), \tag{18}$$

where z is the height above the snow surface, z_0 the surface roughness length of snow (set to 0.001 m in CLASSIC), κ the von Kármán constant, and U_* the friction velocity (constant for the same wind field). The ratio of wind speeds at two heights can be expressed as:

$$\frac{U(z_2)}{U(z_1)} = \frac{\ln(z_2/z_0)}{\ln(z_1/z_0)} \tag{19}$$

Therefore, to calculate the wind speed at 2 m above the snow surface, the following equation is used:

$$U(2) = U(z)\frac{\ln(2/z_0)}{\ln(z/z_0)}, \tag{20}$$

with $z = z_{\text{ground}} - d_s$ where z_{ground} is the reference wind measurement height above the ground, and d_s the snow depth.

The logarithmic wind profile assumes neutral atmospheric conditions. This simplification is common and typically introduces errors of about 10 to 20 % in the surface layer under moderate winds and near-neutral stratification (e.g., Businger et al., 1971; Högström, 1988). Under strongly stable or unstable conditions, deviations can be larger, and Monin–Obukhov similarity theory or more advanced frameworks may be required for greater accuracy (Monin and Obukhov, 1954).

6 CLASSIC spin-up

To perform the CLASSIC spin-up simulations, we cycled through the meteorological forcing files until the carbon pools reached equilibrium (while keeping other forcings constant, such as atmospheric CO_2 concentrations and land cover). To this end, four variables were monitored: the carbon mass flux out of the atmosphere due to net primary production on land (*NPP*), the natural flux of CO_2 from the atmosphere to the land (*NEP*), the net mass flux of carbon from the atmosphere into the land (*NBP*), and the carbon mass in the full depth of the soil model (*cSoil*). The spin-ups were performed until a 10-year average equilibrium state close to 0 was reached for the ratio *NEP* to *NPP* and *NBP*, and *cSoil* reached an asymptote value. CLASSIC allows the soil carbon pool to be spun up faster with the *spinfast* parameter (but without checking carbon conservation). Therefore, a final spin-up phase was run with the *spinfast* parameter set to 1. The first spin-up phase was performed at all sites with the *spinfast* parameter set to 10 over 100 to 300 years (the equilibrium state generally took longer to reach in cold Arctic

regions), and a final spin-up was then performed over the same duration with the *spinfast* parameter set to 1. During the spin-up phases, the CO_2 concentration was held constant at the value corresponding to the first year of the meteorological forcing file specific to each station. An example is shown for Col de Porte in Fig. S2.

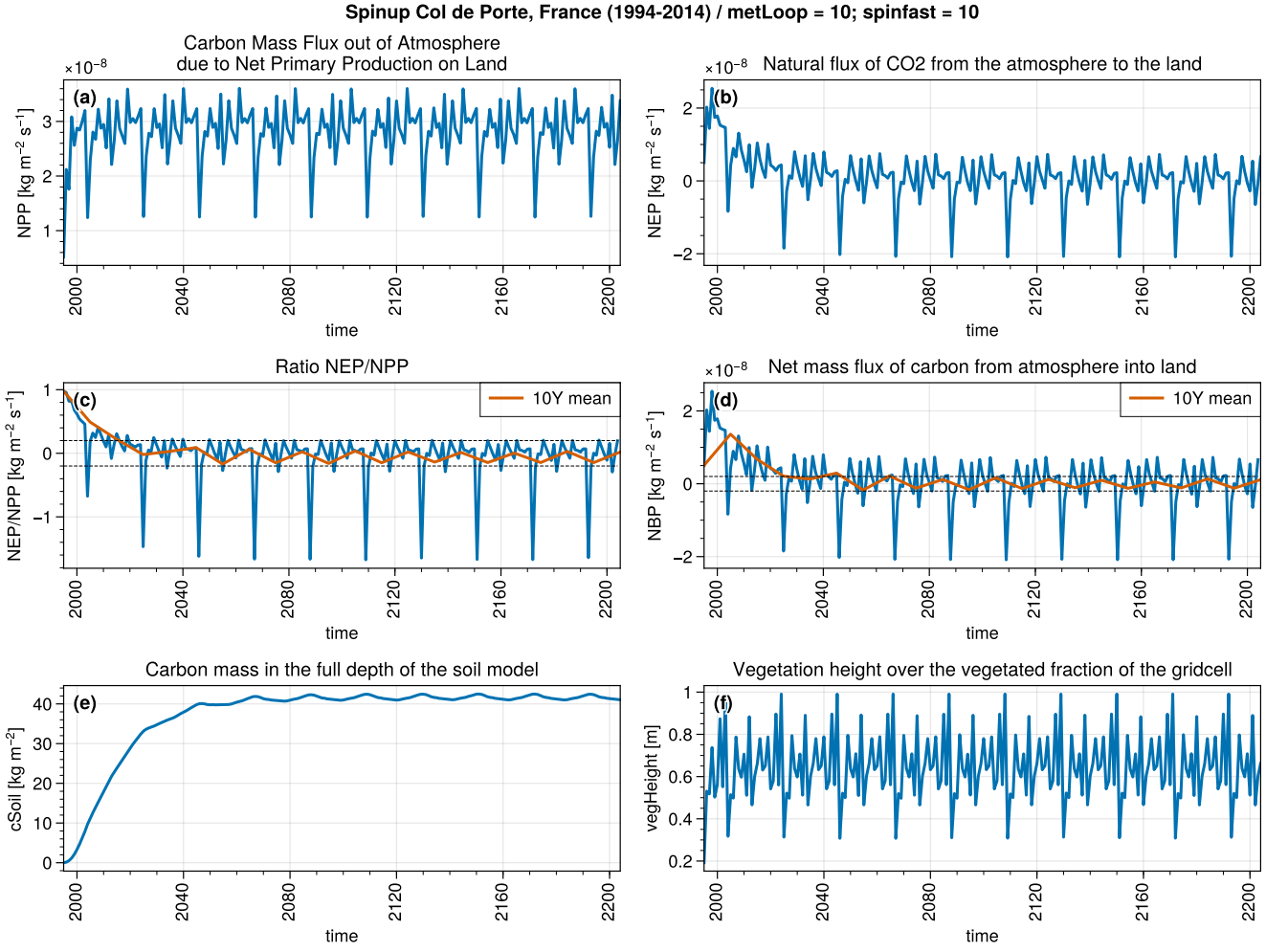

Figure S2. Spin-up annual time series of the *NPP* (a), *NEP* (b), the ratio *NEP* to *NPP* (c), *NBP* (d), *cSoil* (e), and the vegetation height (f) at Col de Porte. The orange lines correspond to the 10-year means on panels (c) and (d), and the dashed lines to the ± 0.2 kg m^{-2} s^{-1} (with a factor 10^{-9} on panel (d)).

7 Issue with the vegetation and albedo

Figure S3 (third column) illustrates the differences between the simulated total grid cell albedo and the simulated snow albedo (Fig. 3; third column in the main text), which are primarily caused by vegetation protruding above the snow. This effect varies across sites, and the simulated vegetation height may differ from observed values.

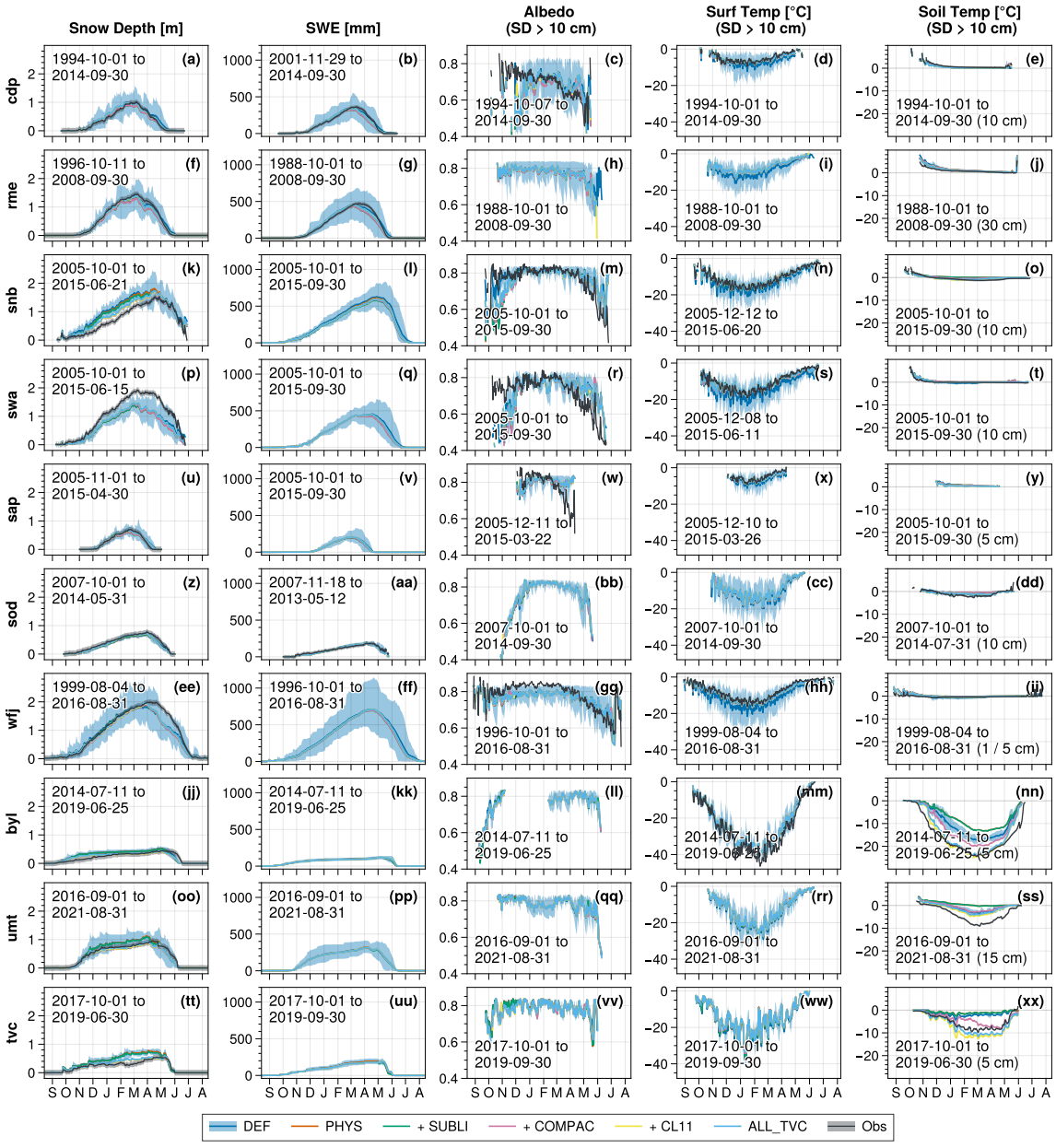

Figure S3. Same as Fig. 3, except for the total grid cell albedo in the third column instead of the snow albedo.

8 Volumetric water content at the Arctic sites

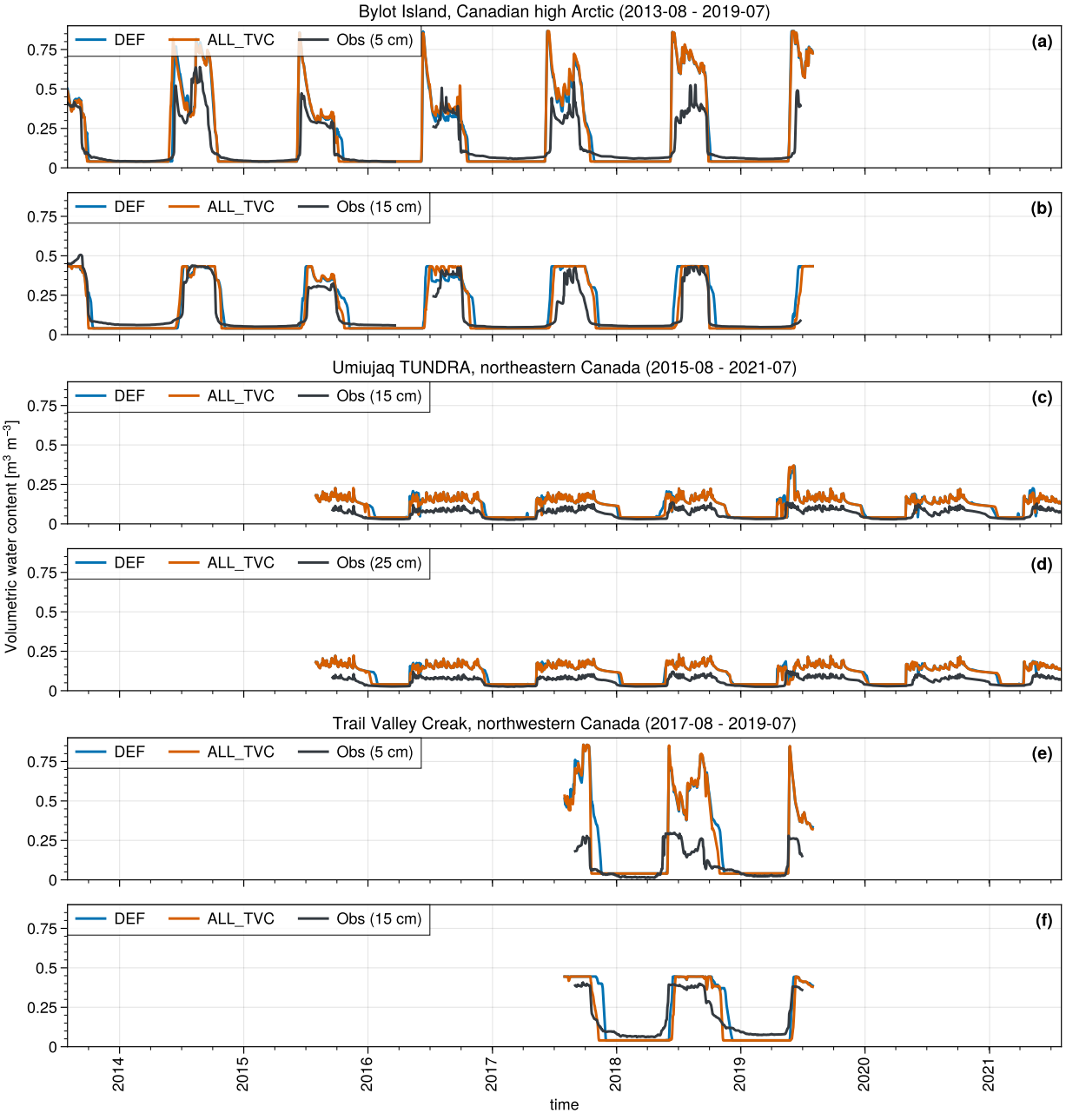

Figure S4. Time series of volumetric water content at the two first measured levels at Bylot (a, b), Umiujaq TUNDRA (c, d), and TVC (e, f) for the *DEF* (blue) and *ALL_TVC* (orange) experiments and the observations (black). When *DEF* experiment (blue line) is not visible, it is superimposed with the *ALL_TVC* experiments (orange line).

9 Arctic winter CO_2 emissions

Soil temperatures play a crucial role in driving winter CO_2 fluxes when the soil is frozen (Mavrovic et al., 2023). Therefore, improving simulated soil temperatures can lead to an improved Arctic winter carbon budget. In this section, we analyze the net ecosystem exchange (NEE)—the net flux of CO_2 between the land surface and the atmosphere—at Bylot, Umiujaq, and TVC. The *DEF* and *ALL_TVC* experiments are analyzed without flux-tower observations (Fig. S5), and compared to observations where available (Fig. S6).

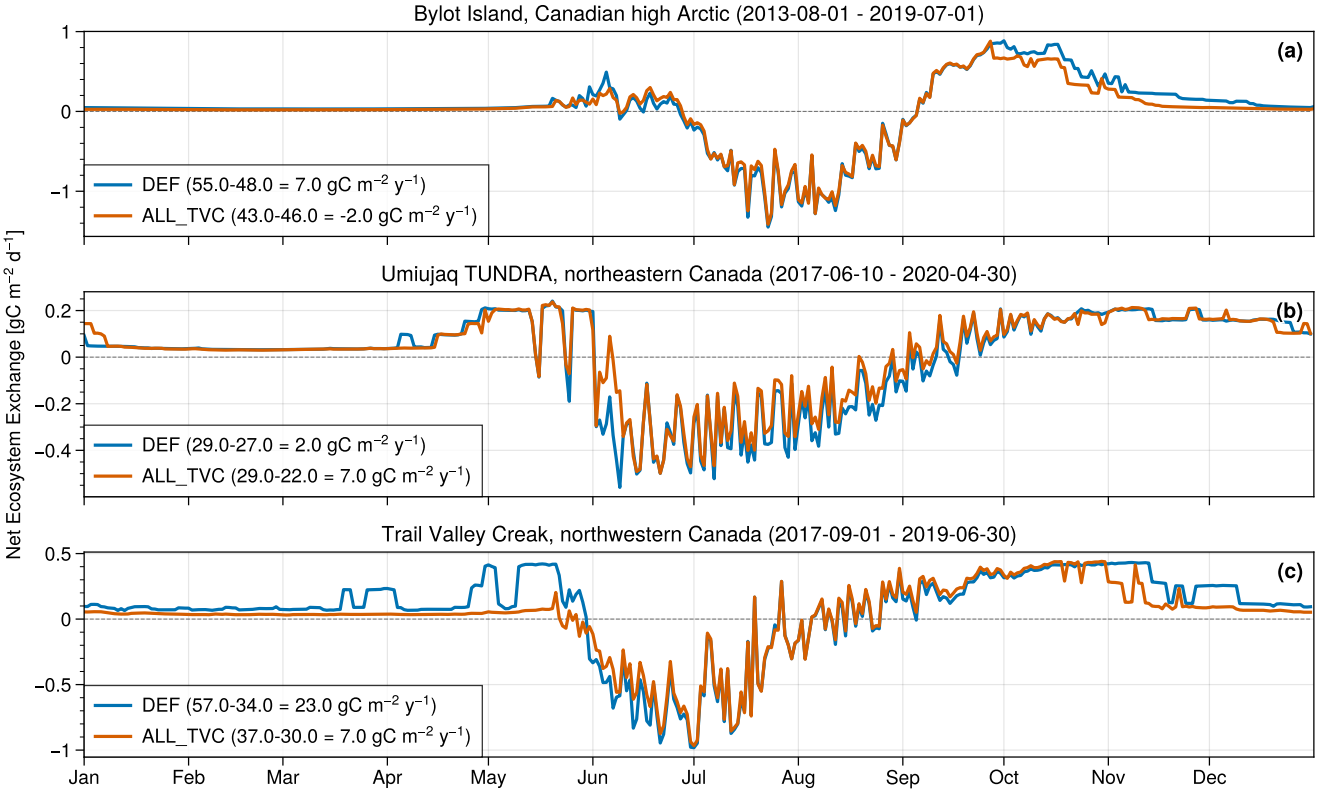

Figure S5. Net ecosystem exchange annual cycles in gC m^{-2} d^{-1} at Bylot (a), Umiujaq TUNDRA (b), and Trail Valley Creek (c). The blue and orange lines correspond to the *DEF* and *ALL_TVC* experiments, respectively, and the black line to the observations. The annual budgets are shown in brackets on the labels with the positive and negative contributions corresponding to net carbon source and sink periods, respectively.

At all the Arctic sites, the ecosystem acts as a carbon sink during the growing season and becomes a carbon emitter from about September to May. The annual budget varies between the *DEF* (blue line) and *ALL_TVC* (orange line) experiments. The new developments included in the *ALL_TVC* experiment reduce the annual NEE at Bylot and TVC from 7.0 (source) to -2.0 (sink) and 23.0 to 7.0 gC m^{-2} y^{-1} respectively (panels a and c). Indeed, the reduced simulated winter soil temperatures in *ALL_TVC* result in lower simulated respiration rates, especially visible at Bylot and TVC during the soil water phase change

periods (spring and autumn). At Umiujaq the changes led to a slight increase in NEE (2.0 to 7.0 gC m^{-2} y^{-1}), indicating that additional factors—such as soil moisture dynamics or plant productivity changes—may also be at play, although the simulated soil temperature changes are much smaller at this site than at to Bylot and TVC (Fig. 3ss in the main text), and the yearly net carbon emission rates remain stable at 29.09 gC m^{-2} y^{-1}.

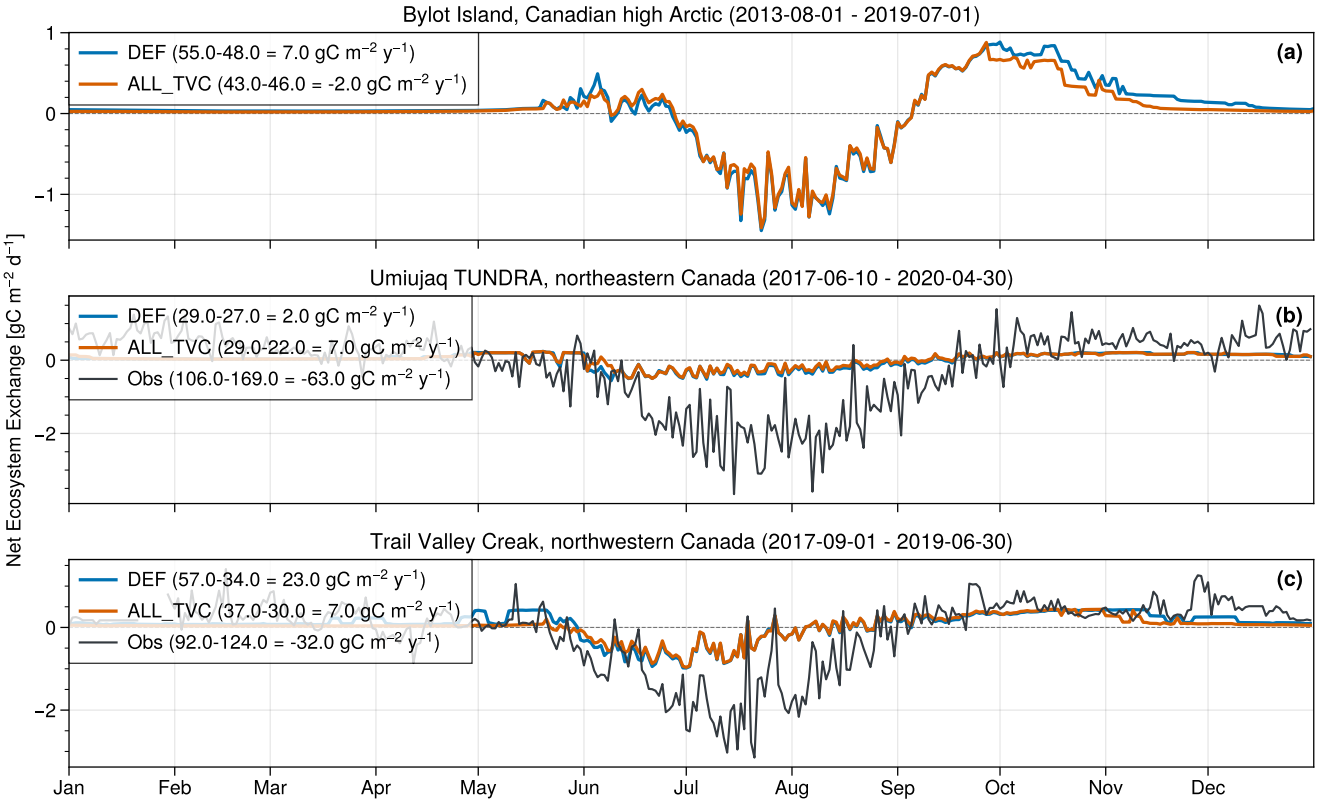

Figure S6. Same as Fig. S5 but with flux-tower observations where available (black line).

The simulated NEE deviates significantly from the observed NEE (Fig. S6 black line), particularly in terms of amplitude, which is much smaller in the simulations. Large uncertainties affect flux tower measurements in winter (Natali et al., 2019), and discrepancies in modeled vegetation cover could contribute to these biases—such as the absence of moss and lichen in CLASSIC. For example, if we prescribe full shrub cover at Umiujaq instead of a 50% shrub–bare ground mix, the simulated carbon fluxes become comparable to observations (not shown). This highlights a key limitation of using a peat layer to indirectly represent moss and lichen in CLASSIC, as it fails to capture the correct carbon dynamics fully. Therefore, further investigation is needed—specifically focusing on carbon flux processes—to better understand the discrepancies between simulated and observed NEE.

10 Boreal SnowMIP sites

The boreal BERMS sites (Bartlett et al., 2006) were excluded from our study to avoid the complexity of interception of snow by trees. We performed simulations at those sites to check that our new model developments did not degrade the model's performance there (not shown). The impacts of our new developments are negligible at all BERMS sites (Old Aspen, Old Jack Pine, and Old Black Spruce; Saskatchewan, Canada), and the model shows good skill in simulating snow depth and soil temperatures compared to the observations, except during some snow seasons where the simulated soil temperatures tend to be too cold (the soil sometimes freezes in the model while it stays close to the 0 °C curtain in the observations), but that was already the case in the *DEF* configuration. Indeed, our new Arctic adaptation model developments are restricted to the bare ground subareas covered with snow (i.e., snow over bare ground or when the snow depth exceeds the vegetation height), and the improved bottom snow temperature and snow thermal conductivity tend to compensate for each other (see Sect. 3.1 in the main text). At Old Aspen, the simulated albedo (above the canopy) tends to be overestimated by about 0.4, which appears to be related to an underestimated plant area index (PAI) falling below a threshold, leading the model to create a bare-ground subarea during winter. Further investigation will be needed to determine whether the PAI threshold in CLASSIC for determining subareal fractions is realistic and/or why the model underestimates PAI relative to observations. Additional work could also be carried out to reevaluate the interception scheme using new datasets at other sites in future studies (e.g., Sicart et al., 2023).

References

Bartlett, P. A., MacKay, M. D., and Verseghy, D. L.: Modified Snow Algorithms in the Canadian Land Surface Scheme: Model Runs and Sensitivity Analysis at Three Boreal Forest Stands, Atmosphere-Ocean, 44, 207–222, https://doi.org/10.3137/ao.440301, 2006.

Brown, R., Bartlett, P., MacKay, M., and Verseghy, D.: Evaluation of Snow Cover in CLASS for SnowMIP, Atmosphere-Ocean, 44, 223–238, https://doi.org/10.3137/ao.440302, 2006.

Businger, J. A., Wyngaard, J. C., Izumi, Y., and Bradley, E. F.: Flux-Profile Relationships in the Atmospheric Surface Layer, 1971.

Calonne, N., Flin, F., Morin, S., Lesaffre, B., du Roscoat, S. R., and Geindreau, C.: Numerical and Experimental Investigations of the Effective Thermal Conductivity of Snow, Geophysical Research Letters, 38, L23 501, https://doi.org/10.1029/2011GL049234, 2011.

Dharmadasa, V., Kinnard, C., and Baraër, M.: Meteorological Control on Snow Depth Evolution and Snowpack Energy Exchanges in an Agro-Forested Environment by a Measurement-Based Approach: A Case Study in Sainte-Marthe, Eastern Canada, Agricultural and Forest Meteorology, 347, 109 915, https://doi.org/10.1016/j.agrformet.2024.109915, 2024.

Dutch, V. R., Rutter, N., Wake, L., Sandells, M., Derksen, C., Walker, B., Hould Gosselin, G., Sonnentag, O., Essery, R., Kelly, R., Marsh, P., King, J., and Boike, J.: Impact of Measured and Simulated Tundra Snowpack Properties on Heat Transfer, The Cryosphere, 16, 4201–4222, https://doi.org/10.5194/tc-16-4201-2022, 2022.

Gagnon, M., Domine, F., and Boudreau, S.: The Carbon Sink Due to Shrub Growth on Arctic Tundra: A Case Study in a Carbon-Poor Soil in Eastern Canada, Environmental Research Communications, 1, 091 001, https://doi.org/10.1088/2515-7620/ab3cdd, 2019.

Gordon, M., Simon, K., and Taylor, P. A.: On Snow Depth Predictions with the Canadian Land Surface Scheme Including a Parametrization of Blowing Snow Sublimation, Atmosphere-Ocean, 44, 239–255, https://doi.org/10.3137/ao.440303, 2006.

Hengl, T., de Jesus, J. M., Heuvelink, G. B. M., Gonzalez, M. R., Kilibarda, M., Blagotić, A., Shangguan, W., Wright, M. N., Geng, X., Bauer-Marschallinger, B., Guevara, M. A., Vargas, R., MacMillan, R. A., Batjes, N. H., Leenaars, J. G. B., Ribeiro, E., Wheeler, I., Mantel, S., and Kempen, B.: SoilGrids250m: Global Gridded Soil Information Based on Machine Learning, PLOS ONE, 12, e0169 748, https://doi.org/10.1371/journal.pone.0169748, 2017.

Högström, U.: Non-Dimensional Wind and Temperature Profiles in the Atmospheric Surface Layer: A Re-Evaluation, Boundary-Layer Meteorology, 42, 55–78, https://doi.org/10.1007/BF00119875, 1988.

Huang, J.: A Simple Accurate Formula for Calculating Saturation Vapor Pressure of Water and Ice, Journal of Applied Meteorology and Climatology, 57, 1265–1272, https://doi.org/10.1175/JAMC-D-17-0334.1, 2018.

Lackner, G., Domine, F., Nadeau, D. F., Lafaysse, M., and Dumont, M.: Snow Properties at the Forest–Tundra Ecotone: Predominance of Water Vapor Fluxes Even in Deep, Moderately Cold Snowpacks, The Cryosphere, 16, 3357–3373, https://doi.org/10.5194/tc-16-3357-2022, 2022.

Lalande, M.: SnowC2-CLASSIC-1D: Model Configuration, Forcing Data, and Simulation Outputs, Zenodo [Data Set], https://doi.org/10.5281/zenodo.18175772, 2026.

Lejeune, Y., Dumont, M., Panel, J.-M., Lafaysse, M., Lapalus, P., Le Gac, E., Lesaffre, B., and Morin, S.: 57 Years (1960–2017) of Snow and Meteorological Observations from a Mid-Altitude Mountain Site (Col de Porte, France, 1325 m of Altitude), Earth System Science Data, 11, 71–88, https://doi.org/10.5194/essd-11-71-2019, 2019.

Marsh, P., Bartlett, P., MacKay, M., Pohl, S., and Lantz, T.: Snowmelt Energetics at a Shrub Tundra Site in the Western Canadian Arctic, Hydrological Processes, 24, 3603–3620, https://doi.org/10.1002/hyp.7786, 2010.

Mavrovic, A., Sonnentag, O., Lemmetyinen, J., Voigt, C., Rutter, N., Mann, P., Sylvain, J.-D., and Roy, A.: Environmental Controls of Winter Soil Carbon Dioxide Fluxes in Boreal and Tundra Environments, Biogeosciences, 20, 5087–5108, https://doi.org/10.5194/bg-20-5087-2023, 2023.

Monin, A. S. and Obukhov, A. M.: Basic Laws of Turbulent Mixing in the Ground Layer of the Atmosphere, Trudy Geofizicheskogo Instituta, Akademiya Nauk SSSR, 24, 163–187, 1954.

Natali, S. M., Watts, J. D., Rogers, B. M., Potter, S., Ludwig, S. M., Selbmann, A.-k., Sullivan, P. F., Abbott, B. W., Arndt, K. A., Birch, L., Björkman, M. P., Bloom, A. A., Celis, G., Christensen, T. R., Christiansen, C. T., Commane, R., Cooper, E. J., Crill, P., Czimczik, C., Davydov, S., Du, J., Egan, J. E., Elberling, B., Euskirchen, E. S., Friborg, T., Genet, H., Göckede, M., Goodrich, J. P., Grogan, P., Helbig, M., Jafarov, E. E., Jastrow, J. D., Kalhori, A. A. M., Kim, Y., Kimball, J. S., Kutzbach, L., Lara, M. J., Larsen, K. S., Lee, B.-y., Liu, Z., Loranty, M. M., Lund, M., Lupascu, M., Madani, N., Malhotra, A., Matamala, R., McFarland, J., McGuire, A. D., Michelsen, A., Minions, C., Oechel, W. C., Olefeldt, D., Parmentier, F.-J. W., Pirk, N., Poulter, B., Quinton, W., Rezanezhad, F., Risk, D., Sachs, T., Schaefer, K., Schmidt, N. M., Schuur, E. A. G., Semenchuk, P. R., Shaver, G., Sonnentag, O., Starr, G., Treat, C. C., Waldrop, M. P., Wang, Y., Welker, J., Wille, C., Xu, X., Zhang, Z., Zhuang, Q., and Zona, D.: Large Loss of CO2 in Winter Observed across the Northern Permafrost Region, Nature Climate Change, 9, 852–857, https://doi.org/10.1038/s41558-019-0592-8, 2019.

Shangguan, W., Hengl, T., Mendes de Jesus, J., Yuan, H., and Dai, Y.: Mapping the Global Depth to Bedrock for Land Surface Modeling, Journal of Advances in Modeling Earth Systems, 9, 65–88, https://doi.org/10.1002/2016MS000686, 2017.

Sicart, J. E., Ramseyer, V., Picard, G., Arnaud, L., Coulaud, C., Freche, G., Soubeyrand, D., Lejeune, Y., Dumont, M., Gouttevin, I., Le Gac, E., Berger, F., Monnet, J.-M., Borgniet, L., Mermin, É., Rutter, N., Webster, C., and Essery, R.: Snow Accumulation and Ablation Measurements in a Midlatitude Mountain Coniferous Forest (Col de Porte, France, 1325 m Altitude): The Snow Under Forest (SnoUF) Field Campaign Data Set, Earth System Science Data, 15, 5121–5133, https://doi.org/10.5194/essd-15-5121-2023, 2023.

Sturm, M., Holmgren, J., König, M., and Morris, K.: The Thermal Conductivity of Seasonal Snow, Journal of Glaciology, 43, 26–41, https://doi.org/10.3189/S0022143000002781, 1997.

Tabler, R. D., Benson, C. S., Santana, B. W., and Ganguly, P.: Estimating Snow Transport from Wind Speed Records: Estimates versus Measurements at Prudhoe Bay, Alaska, in: 58th Annual Western Snow Conference, Proceedings of the 58th Annual Western Snow Conference, Western Snow Conference, Sacramento, California, 1990.

Wang, A., Price, D. T., and Arora, V.: Estimating Changes in Global Vegetation Cover (1850–2100) for Use in Climate Models, Global Biogeochemical Cycles, 20, GB3028, https://doi.org/10.1029/2005GB002514, 2006.